J Nanopart Res (2016) 18: 345
DOI 10.1007/s11051-016-3646-0

RESEARCH PAPER

Cell viability and MRI performance of highly efficient polyol-coated magnetic nanoparticles

Fernando Arteaga-Cardona · Eric Gutiérrez-García · Silvia Hidalgo-Tobón · Ciro López-Vasquez · Yazmín A. Brito-Barrera · Julia Flores-Tochihuitl · Aracely Angulo-Molina · Julio R. Reyes-Leyva · Roberto González-Rodríguez · Jeffery L. Coffer · Umapada Pal · Mario Pérez-Peña Diaz-Conti · Diana Platas-Neri · Pilar Dies-Suarez · Rebeca Sosa Fonseca · Oscar Arias-Carrión · Miguel A. Méndez-Rojas

Received: 18 June 2016 / Accepted: 25 October 2016 / Published online: 21 November 2016

Abstract This work aimed at determining conditions that would allow us to control the size of the NPs and create a system with characteristics apt for biomedical applications. We describe a comprehensive study on the synthesis and physical characterization of two highly sensitive sets of triethylene glycol (TREG) and polyethylene glycol (PEG)-coated superparamagnetic iron oxide nanoparticles (SPIONs) to be evaluated for use as magnetic resonance (MR) contrast agents. The ferrofluids demonstrated excellent colloidal stability in deionized water at pH 7.0 as indicated by dynamic light scattering (DLS) data. The magnetic relaxivities, r_2, were measured on a 1.5 T clinical MRI instrument. Values in the range from 205 to 257 mM^{-1} s^{-1} were

Electronic supplementary material The online version of this article (doi:10.1007/s11051-016-3646-0) contains supplementary material, which is available to authorized users.

F. Arteaga-Cardona · C. López-Vasquez · Y. A. Brito-Barrera · M. A. Méndez-Rojas (✉)
Departamento de Ciencias Químico-Biológicas, Universidad de las Américas de Puebla, Sta. Catarina Mártir s/n, C.P. 72810 San Andrés Cholula, Puebla, Mexico
e-mail: miguela.mendez@udlap.mx

E. Gutiérrez-García
Universidad Autónoma del Estado de México, Instituto Literario, # 100. Col. Centro, C.P. 50000 Toluca, Mexico

S. Hidalgo-Tobón (✉) · R. S. Fonseca
Departamento de Física, Universidad Autónoma Metropolitana, Avenida San Rafael Atlixco 186 Iztapalapa, México City, Mexico
e-mail: shid@xanum.uam.mx

S. Hidalgo-Tobón · M. P.-P. Diaz-Conti · P. Dies-Suarez
Hospital Infantil de México Federico Gómez, Dr. Márquez 162, Col. Doctores, C.P. 06720 México City, Mexico

J. Flores-Tochihuitl
Facultad de Estomatología, Benemérita Universidad Autónoma de Puebla, 31 Poniente 1304, Col. Volcanes, C.P. 72400 Puebla, Puebla, Mexico

A. Angulo-Molina
Departamento de Ciencias Químico-Biológicas, Universidad de Sonora, Blvd. Luis Encinas y Rosales s/n, Col. Centro, C.P. 83000 Hermosillo, Sonora, Mexico

J. R. Reyes-Leyva
Centro de Investigación Biomédica de Oriente (CIBIOR), Instituto Mexicano del Seguro Social, C.P. 74360 Metepec, Puebla, Mexico

R. González-Rodríguez · J. L. Coffer
Department of Chemistry, Texas Christian University, Box 298860, Fort Worth, TX 76129, USA

obtained, varying proportionally to the SPIONs' sizes and coating nature. Further in vitro cell viability tests and in vivo biodistribution analyses of the intravenously administered nanoparticles showed that the prepared systems have good biocompatibility and migrate to several organs, mainly the meninges, spleen, and liver. Based on these results, our findings demonstrated the potential utility of these nanosystems as clinical contrast agents for MR imaging.

Keywords Magnetite · Nanoparticles · MRI · Relaxivity · Cell viability · Biodistribution

Introduction

Superparamagnetic iron oxide nanoparticles (SPIONs) are of great interest due to their potential applications in diverse fields such as biomedicine, bioseparation, biotechnology, and in catalysis, (Rojas-Perez et al. 2015; Beltran-Huarac et al. 2013; Zhang et al. 2013; Engelhardt et al. 1994; He et al. 2012; Papakonstantinou et al. 1995; Wang et al. 2009; Zhang et al. 2008) not only because of their excellent magnetic response but also their low toxicity and biosafety. These entities usually have a magnetic nanoparticle as the core, surrounded by a hydrophilic and biocompatible coating.

Hydrophilic SPIONs are ideal nanomaterials that, when coupled with appropriate surface chemistry applications, can be used for numerous biomedical in vivo applications such as magnetic separation, drug delivery, cancer hyperthermia, and magnetic resonance imaging (MRI) contrast enhancement (Pankhurst et al. 2003; Mornet et al. 2004). The use of superparamagnetic nanoparticles as contrast agents in MRI has been a major development in the range of tools available to clinicians. SPIONs have attracted an increasing interest in the last 10 years because they can produce enhanced relaxation rates in specific organs at significantly lower doses (mmol/kg) than paramagnetic ions, due to their larger magnetic moment (Merbach et al. 2001).

All of the abovementioned biomedical applications require the nanoparticles to be non-toxic (Weissleder et al. 1989), water soluble, superparamagnetic, have high magnetization values and chemical stability, a size smaller than 100 nm, narrow particle size distribution, and be easy to produce on a large scale. The synthesis of magnetite particles that can meet all these requirements remains a challenge.

It has been demonstrated that the physical and chemical properties of magnetite nanoparticles greatly depend on the synthesis route (Masala and Seshadri 2005; Ammar et al. 2001). The size and morphology of the nanoparticles (NPs) can be controlled by adjusting pH, reaction temperature, precursor, and the Fe(II)/Fe(III) concentration ratio (Ali et al. 2016).

The control of the monodisperse size is crucial because the properties of the nanocrystals strongly depend upon the dimension of the nanoparticles. Iron oxide nanoparticles become superparamagnetic when their size is under 20 nm (Issa et al. 2013). This characteristic is important for their biomedical applications as magnetization ceases after the removal of the external magnetic field, avoiding undesirable in vitro or in vivo aggregation (Yang et al. 2013). Furthermore, magnetic nanoparticles with diameter sizes under 8–10 nm (USPIONs, ultrasmall superparamagnetic iron oxide nanoparticles) have longer retention time in blood, avoid clearance by the reticuloendothelial system (RES), and can reach other tissues and organs, besides the liver (Bourrinet et al. 2006; Lind et al. 2002; Weissleder et al. 1990). Also, their small size allows for sub-cellular targeting which can overcome certain physical barriers that larger molecules such as pharmaceutical drugs may not (Zhu and Torchilin 2013).

One of the most popular ways to prepare high-quality water-stable SPIONs is polyol-mediated synthesis. This simple, low-cost method uses high-boiling solvents such as triethylene glycol (TREG) (Wei and Wan 2007; Mondini et al. 2008) and poly(ethylene glycol) (PEG) (Mondini et al. 2008) that allow for the high temperatures needed for decomposition of the chemical precursor. Because of the reaction environment used, this method produces SPIONs with a hydrophilic coating (a desirable characteristic to retard detection and

U. Pal
Instituto de Física, Benemérita Universidad Autónoma de Puebla, Apdo, Postal J-48, C.P. 72570 Puebla, Pue, Mexico

D. Platas-Neri
Escuela de Estudios Superiores del Jicarero, Universidad Autónoma del Estado de Morelos, Carr. Galeana-Tequesquitengo s/n, Jojutla, C.P. 62909 Morelos, Mexico

O. Arias-Carrión
Trastornos del Movimiento y Sueño (TMS), Hospital General Dr. Manuel Gea González, Av. Calzada de Tlalpan 4800, Col. Sección XVI, C.P. 14080 México City, Mexico

removal by the RES) (Wang 2011), acceptable size uniformity, and good crystallinity, making them useful for many applications. Another advantage of this simple one-step method is that the polyol-coated magnetic nanoparticles are highly soluble in aqueous solvents and biocompatible (Joseyphus et al. 2010). Furthermore, the cost of their manufacture is lower than nanostructures obtained by other techniques which require additional steps for surface functionalization.

The biodistribution, cell viability, and MRI performance of polyol-coated magnetic nanoparticles have recently been reviewed in several publications (Miguel-Sancho et al. 2011; Xue et al. 2015; Hachani et al. 2016). However, to our knowledge, most of these studies focus exclusively on the preparation and characterization of magnetic nanoparticles, or the evaluation of their cytotoxicity in a cell culture or animal model, or the in vitro performance analysis as MRI contrast agent. As these aspects were assessed separately, their work misses the chance to make a holistic study of this nanomaterial.

In this work, we report a comprehensive study on the preparation and characterization of TREG and PEG-coated SPIONs with controlled sizes and enhanced magnetic properties, as well as the MRI performance both in vitro and in vivo and biological testing conducted on one of these systems. The results indicate that the magnetic nanoparticles have appropriate tissue biodistribution, are biocompatible, and show excellent performance as potential clinical MRI contrast agents (CAs).

Experimental

All the chemicals were purchased from commercial sources and were reagent grade unless otherwise indicated. Iron (III) acetylacetonate, [Fe(acac)$_3$] (97%, Aldrich), was used as iron oxide precursor and thermally decomposed at high temperatures in both triethylene glycol (TREG, 99%, Aldrich) and polyethylene glycol-6000 (PEG_{6000}, premium, Aldrich). The main function of the polyol in the synthesis is contributing to the partial reduction of Fe^{3+} to Fe^{2+}, in the appropriate stoichiometry to yield $Fe_3(OH)_8$ which turns into magnetite (Fe_3O_4) after thermal decomposition. The polyol also serves as a high-boiling point solvent and surfactant that prevents aggregation by maintaining the size of the nanoparticles uniform as they grow (Joseyphus et al. 2010). In this work, magnetite nanoparticles were prepared following a method similar to that proposed by Cai et al., but without using an inert atmosphere. Nanoparticles obtained through this method were about 9 nm in diameter on average (Cai and Wan 2007).

Preparation of TREG-coated Fe_3O_4 nanoparticles

Fe_3O_4@TREG-1 (TREG-1): In a typical synthesis, 25 mL (186.4 mmol) of TREG and 1.412 g (4 mmol) of [Fe(acac)$_3$] were mixed in a 100-mL round bottom flask equipped with a condenser, magnetic stirrer, heating nest, rheostat, thermocouple, and heated until the temperature reached 453 K. The temperature was maintained for about 30 min, until the solution turned darker. The temperature of the reaction mixture was then increased rapidly to 553 K and maintained for another 30 min. The solution turned a dense black and responded positively to an external magnetic field. The reaction mixture was slowly cooled down to room temperature, and the product was washed three times with a mixture of ethyl acetate (40 mL) and ethanol (10 mL). A permanent Nd magnet at the bottom of the flask induced precipitation of the product, and the solid particles were then recovered by decantation. The final product, a black magnetic powder (Fe_3O_4 nanoparticles), was dried under vacuum at room temperature and then stored in a freezer (277 K).

Fe_3O_4@TREG-2 (TREG-2): TREG-2 was prepared following the same procedure used for TREG-1, but by changing the volume of TREG (the concentration of the iron precursor in the reaction mixture) and modifying the temperature and heating time at different stages as shown in Table 1.

Preparation of PEG-coated Fe_3O_4 nanoparticles

This synthesis was realized with some modifications of a method reported by Zhang (Zhang et al. 2008). Carboxylation of PEG was achieved by the oxidative carboxylation of PEG_{3400} as reported by Fishman (Fishman et al. 2004).

Fe_3O_4@PEG-1 (PEG-1): 0.8 g (2.264 mmol) of [Fe(acac)$_3$] and 1.0 g (0.166 mmol) of carboxylated PEG were mixed in a 100-mL round bottom flask, same as the one described earlier. The mixture was heated to 473 K and maintained at this temperature for 30 min. After this time, the temperature was rapidly raised to 533 K and sustained for another 40 min. A change in

Table 1 Polyol-coated magnetic nanoparticle preparation conditions and resulting NP sizes

Condition	TREG-1	PEG-1	TREG-2	PEG-2
[Fe(acac)$_3$]	1.41 g (4.0 mmol)	0.80 g (2.26 mmol)	0.35 g (1 mmol)	0.80 g (2.26 mmol)
Polyol (PEG or TREG)	25.0 mL (186.4 mmol)	1.0 g (0.166 mmol)	9.4 mL (70 mmol)	0.75 g (0.125 mmol)
Temperature, time (K, min) (1st stage)	453, 30	473, 30	453, 60	473, 60
Temperature, time (K, min) (2nd stage)	553, 30	533, 40	523, 60	533, 80
Average size (nm) (DLS)	20	20	40	180
Average size (nm) (TEM)	6	8	12	14

color of the solution from reddish to black indicated the completion of the reaction. The black suspension was cooled to room temperature, and the solid product was dispersed in 70 mL of ether/acetone (3:3 *v*/*v*) mixture to remove impurities and any unreacted precursor. Finally, the product was magnetically decanted, dried at room temperature, and stored at 277 K. The derived product is a black powder with an intense magnetic response and good solubility both in water and ethanol.

Fe_3O_4@PEG-2 (PEG-2): PEG-2 was made following the same procedure used for preparing PEG-1, but by changing the volume of PEG and the heating time for stages 1 and 2, as indicated in Table 1.

Characterization

Transmission electron microscope (TEM) images were obtained on a JEOL J-2100 (JEOL USA, Inc., Peabody, MA) electron microscope at an acceleration voltage of 200 kV. TEM samples were prepared by placing one drop of a dilute suspension of magnetite nanoparticles in water on carbon-coated copper grids and allowing the solvent to evaporate at room temperature. The average particle size (D_{TEM}) and size distribution were evaluated by measuring the largest internal dimension of 100 particles. Powder X-ray diffraction (XRD) measurements were taken of the dry, ground powder in a quartz sample holder in a Bruker D8 Advance (Bruker AXS Inc., Madison, Wisconsin, USA,) diffractometer using the Cu $K_{\alpha 1}$ line source (λ = 1.54018 Å) in 2θ mode (measuring interval 10 to 90°); scan step = 0.02°; time step = 0.6 s. Hydrodynamic particle diameter and particle size distribution were determined via dynamic light scattering using a Nanotrac Wave system (Microtrac Inc., Montgomeryville, PA, USA) analyzer, with a red laser of 780 nm, 3 mW. Fourier transform infrared (FTIR) spectra were recorded for finely ground dry powder samples on a Varian-Scimitar FTIR-800 (Varian, Palo Alto, CA., USA) spectrophotometer equipped with an ATR detector in the spectral range 4000–800 cm^{-1}.

Fe content determination

An adaptation of the method reported by Wang et al. for the spectrophotometric determination of Fe(II) was used to determine the Fe content (Rohani Moghadam et al. 2015; Wang et al. 1982). Briefly, the UV-visible absorption spectra of an iron(II) complex with 1,10-phenantroline (>99%, Aldrich) was determined using a UV-Vis Cary 100 (Varian, Palo Alto, CA, USA) spectrophotometer. For this purpose, 10 mg of the polyol-coated SPIONs was dissolved in 10 mL of HCl (6 M, 37%, ACS reagent) under sonication for 20 min. Then, 1 mL of a 10% hydroxylamine hydrochloride (98%, ACS reagent) solution was added to reduce all Fe(III) to Fe(II). Then, 8 mL of sodium acetate buffer (pH 5.2 ± 0.1, Sigma) and 5 mL of a 1,10-phenanthroline 4.8 mM solution were added and stirred vigorously. Almost immediately, an intensely orange colored complex [Fe(phen)$_3$]$^{2+}$ formed. After 15 min, the solution was diluted to 100 mL by adding deionized water and the absorbance of the sample measured at 508 nm. The concentration of iron in each sample was estimated utilizing a previously prepared calibration curve.

Magnetic resonance relaxometry

MR relaxometry of the magnetic nanoparticles was measured using a clinical 1.5 T whole body MRI scanner (Philips Intera-Achieva, Philips Healthcare, Best, Netherlands). Four SPION samples (TREG-1, PEG-1, TREG-2, and PEG-2) were dispersed in a mixture of

distilled water and 0.3 g of agar gel at iron concentrations in a range from 4.3 to 64.2 μg/mL for PEG-coated nanoparticles and from 5.7 to 28.0 μg/mL for TREG-coated nanoparticles in plastic tubes (15 mL). Images were taken in 2D mode with a mFFE (multi fast field echo) sequence, maximum gradient amplitude of 80 mT/m, a slew rate of 120 mT/m/ms, an 8-channel SENSE head coil, TR/TE = 230/46 ms, slice thickness of 5 mm and NEX = 2, angle flip = 18 and echo times TE = 0, 20, 40, 60, 80, and 100 ms, at the same spatial position (Fig. 5). For each sample, T_2-weighted images of the samples for three different Fe concentrations (TREG-1 5.7, 11.0, 20.7; PEG-1 4.3, 6.4, 14.3; TREG-2 9.4, 13.3, 28.0; PEG-2 22.5, 32.1, 64.2 μg/mL) were obtained. The relaxation time T_2 was obtained from the MR images by fitting the measured signal intensity decay into an exponential curve (Eq. 1) (Arteaga-Cardona et al. 2016b). To determine the changes induced by the magnetic nanoparticles on the water's ^{1}H protons relaxometry, the average signal strength provided by each MRI image at a specific TE was measured using OsiriX (2004). This data was then fitted into an Eq. (1), obtaining the T_2 value and finally, calculating r_2 from $r_2 = 1/T_2$.

$$S_{SE} = S_0 e^{-\frac{TE}{T2}} \quad (1)$$

where S_{SE} represents the intensity of the signal at a defined echo time, and S_0 is the original intensity of the signal without the magnetic material.

Magnetic measurements

The magnetic properties of samples TREG-2 and PEG-2 were measured using a vibrating sample magnetometer (VSM) attached to a Physical Property Measurements System (PPMS, Quantum Design, Dyna-cool 9, USA). The samples were subjected to different magnetic field strengths (H), and the induced magnetization (M) was measured at three temperatures (300, 100, and 10 K). The external magnetic field was reversed on saturation, and the hysteresis loop was traced.

Cell viability test

Mouse fibroblast cells (ATCC No. CCL-1) used in this study were provided by CIAD (Centro de Investigación en Alimentación y Desarrollo, Sonora, México). The cells were cultured in Dulbecco's modified Eagle's medium (DMEM, Sigma) supplemented with 5% fetal bovine serum (FBS, Sigma), 1% penicillin-streptomycin (Sigma), and 1% glutamine (Sigma) at 310 K in a humidified atmosphere with 5% CO_2. TREG-2 and PEG-2 SPIONs were sterilized by filtration through 0.45 μm Millex CV filter units (Millipore), and their effects on cell viability/cytotoxicity were determined using the MTT (3-[4,5-dimethylthyazol-2-yl]-2,5 diphenyl tetrazolium bromide, 98%, Sigma) colorimetric assay. Fibroblasts (1.0×10^4 cells/well) were seeded in 96-well plates and cultured in a humidified atmosphere with 5% CO_2 at 310 K during 24 h. After that, the medium was replaced with fresh medium containing different concentrations of nanoparticles (0, 1.25, 2.5, 5, 10, 20, 40, 80, and 160 μg/mL) and further incubated for 24, 48, and 72 h. After this time, the medium containing unbound compounds was removed, and MTT solution (5 mg/mL in PBS pH 7.4) was added to all the wells. After further incubation in the dark for 4 h at 310 K, 100 μL of acidified isopropanol was added to each well and the absorbance was monitored in a microplate reader at a wavelength of 550 nm (Jiang et al. 2013). All the tests were performed in triplicate; untreated cells were used as controls, and the cell viability was calculated as follows:

$$\%\text{Cell viability} = (\text{Absorbance of sample well}/\text{absorbance of control well}) \times 100.$$

No evaluation of PEG or TREG toxicity was performed as both are stable, biocompatible hydrophilic polymers that are currently used in many drugs and gene delivery applications (Pisciotti et al. 2016); (Hachani et al. 2016).

In vivo MR imaging experiments

The animal model consisted of a 5-kg New Zealand rabbit kept under appropriate care in the Animal Research Unit of the institution, following the *Guide for the Care and Use of Laboratory Animals*, with approval of the Ethics Committee of Hospital Infantil de Mexico and in accordance with the Mexican Official Norm (NOM) NOM-039 and NOM-062-ZOO-1999 (2011). The study was performed using an 8-channel SENSE head coil on a 1.5 T clinical whole body scanner (Philips Intera-Achieva, Philips Healthcare, Best, Netherlands). Images were taken in 2D mode with a

mFFE sequence, with the following parameters: FOV = 150 mm, matrix 256 × 256, TR = 2348 ms, slice thickness 3 mm, gap = 4 mm, NEX = 2, flip angle = 18, pixel bandwidth pBW = 934 Hz, TE = 4.6, 24.6, 44.6, 64.6, 84.6 ms, maximum gradient amplitude equal to 80 mT/m and a slew rate of 120 mT/m/ms. A suspension of 0.175 mg of TREG-2, containing the equivalent to 50 mg of Fe dispersed in 5 mL of saline solution, was injected intravenously into a vein in the rabbit's right ear. MRI was performed before injection and every day for 3 days after injection of the nanoparticles. Contrast effects were examined in all of the major organs.

Histology

To further verify the MRI results, the animal was sacrificed for histopathological analysis. The brain, meninges, liver, kidneys, intestines, lungs, esophagus, and spleen tissues of the rabbit were treated with 5 mg/mL TREG-2 magnetic nanoparticles, washed with PBS buffer (pH = 7.4), fixed with 4% formaldehyde, and included in paraffin. The tissues were processed with a Leica-Lipshaw EG1150 (Leica Microsystems, Wetzlar, Germany) modular tissue-embedding center, and then cut into histological slices (5 μm) and stained with Prussian blue (Perls staining) for the detection of free exogenous iron. The counterstaining was done with hematoxylin-eosin. All the sections were examined with an optical microscope (Zeiss Axio Scope. A1, Germany).

Results and discussion

The polyol method has been used by several research groups for the preparation of highly monodispersed SPIONs (Cai et al. He et al. 2012). Typically, it consists of two heating stages, one (the activation step) which achieves thermal decomposition of a small fraction of the polyol and yields a reducing agent (formaldehyde) and a second heating stage (the magnetite formation step) where the magnetic iron oxide is formed by the thermal decomposition of the iron precursor. The specific temperature and reaction time of each stage, as well as the nature of the polyol and the concentration of the precursors, are all factors that influence the final size, structure, and morphology of the nanoparticles. Table 1 presents a summary of the preparation conditions for the four samples along with their size, as determined by dynamic light scattering (DLS) and TEM. Products with the desired characteristics were formed only when the temperature of the second heating step was within the 523–553 K range for TREG and 533 K for PEG. Varying the reaction time resulted in nanoparticle formation of different sizes. For example, doubling the time (from 30 to 60 min) in the activation step and in the second step (30 to 60 min, for TREG; 40 to 80 min for PEG) doubled the hydrodynamic radii from 20 to 40 nm for both TREG-coated nanoparticles, and caused an appreciable increase of size for PEG-coated nanoparticles. The observed change in size of the nanoparticles can be attributed to an increase of the iron core diameter, which was confirmed by spectrophotometric estimation of their iron content (almost twice the initial mass of iron for sample TREG-2 compared to TREG-1 and the nearly the same ratio for sample PEG-2 with respect to PEG-1). All samples are black, magnetic powders that are highly dispersible in water. The spectrophotometric determination of iron in 10.0 mg of each of the samples yielded 13.8% of total iron for sample TREG-1, 8.6% for sample PEG-1, 38.5% for sample TREG-2, and 16.0% for sample PEG-2. Those values correspond, respectively, to 86.2, 91.4, 61.5, and 84.0 wt% of the corresponding polyol for TREG-1, PEG-1, TREG-2 and PEG-2, respectively. In this work, the temperature of the first heating step was fixed at 453 K for TREG and 473 K for PEG. Irrespective of the duration of this first step, heating the mixture at lower temperatures produced undesirable products, without magnetic response. The same happened if the initial thermal activation step was missed or shortened. The selection of an appropriate temperature for the second heating stage also seems to be crucial to obtain a product with the desired characteristics.

Characterization of the SPIONs The control of the monodisperse size is vital as the properties of the nanocrystals are strongly dependent on the dimension of the nanoparticles. It has been reported that magnetic nanoparticles smaller than 10 nm are easily removed by renal clearance (Wahajuddin and Sumit 2012). Figure 1 shows typical TEM images of the as-prepared TREG-1, TREG-2, as well as for PEG-1 and PEG-2 samples. Formation of quasi-spherical particles with a size range between 6 to 14 nm (depending on the sample) is very

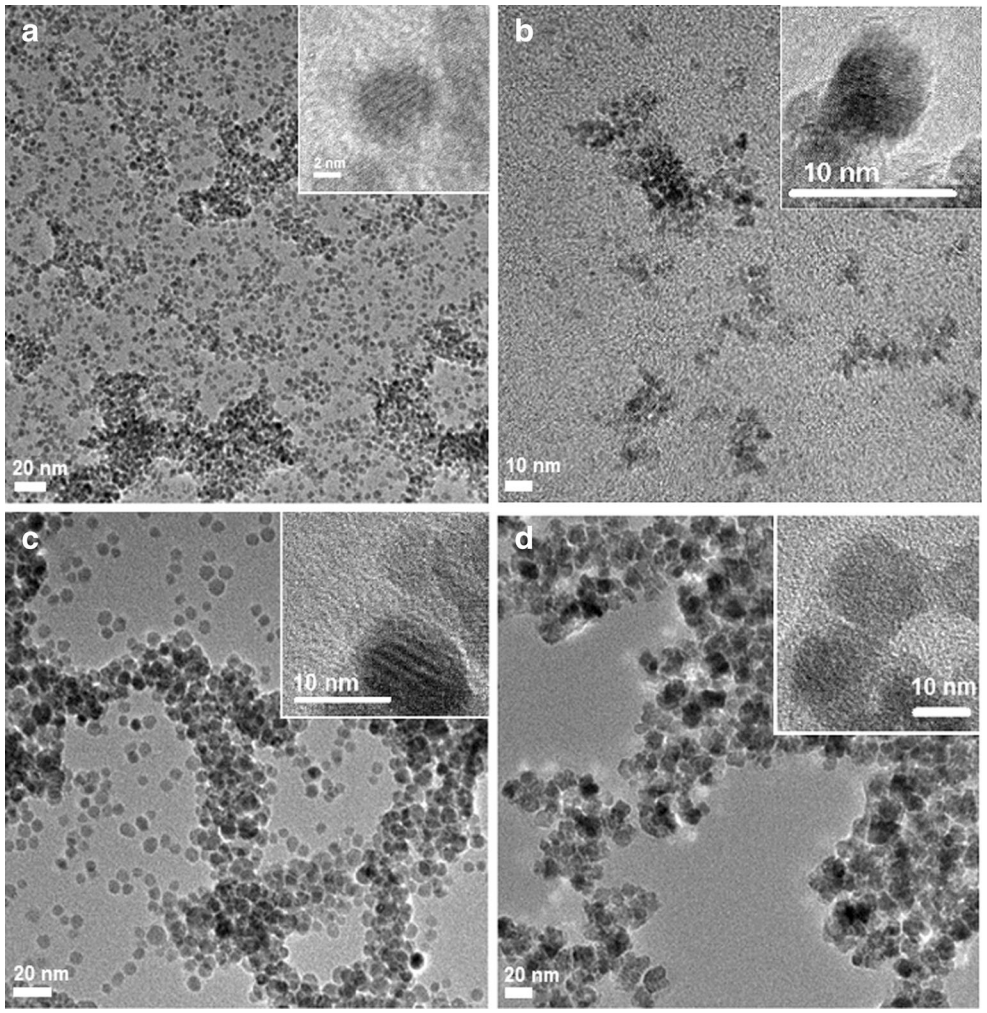

Fig. 1 Typical TEM images of the sample. **a** TREG-1. **b** PEG-1. **c** TREG-2. **d** PEG-2. *Insets* are magnifications of representative particles in each case

clear in the micrographs. The SPIONs are highly crystalline as observed from their selected area electron diffraction (SAED) patterns (see Supplementary Information1).

Size distribution of Fe_3O_4-NPs was determined by DLS, using a Nanotrac Wave Analyzer, at a concentration of 100 ppm in water, at 294 K. The distribution graphs of the SPIONs that were freshly dispersed in DI water with an ultrasonic probe (5 s, Ultrasonic Processor Vibra Cell, Model VC130PB) are shown in the Supplementary Information. The hydrodynamic diameter (HDD) values determined for TREG-1, TREG-2, PEG-1, and PEG-2 are 20, 40, 20, and 180 nm, respectively. These sizes concur with the observed size increases that result from doubling the reaction time (as determined by TEM), with the exception of the large size increases measured for PEG-2 (HDD of 180 nm). This increment may be related to the hydrophilic nature of $PEG_{6000,}$ forming a swollen shell; it has been reported that large molecular weight PEG-coated magnetic nanoparticles are more suitable for agglomeration than their corresponding low-molecular weight counterparts (Yallapu et al. 2010). All samples show excellent colloidal stability in water at pH 7.0, making them appropriate for biomedical applications. The crystalline phase for two selected samples was determined by XRD. Figure 2 shows the XRD patterns for TREG-1 (Fig. 2a) and PEG-1 (Fig. 2b) samples. The XRD patterns show that the nanoparticles are well-crystalline, and the position and relative intensity of the diffraction peaks correspond to the crystalline planes of magnetite (Fe_3O_4, JCPDS 19–0629). Finally, the presence of the

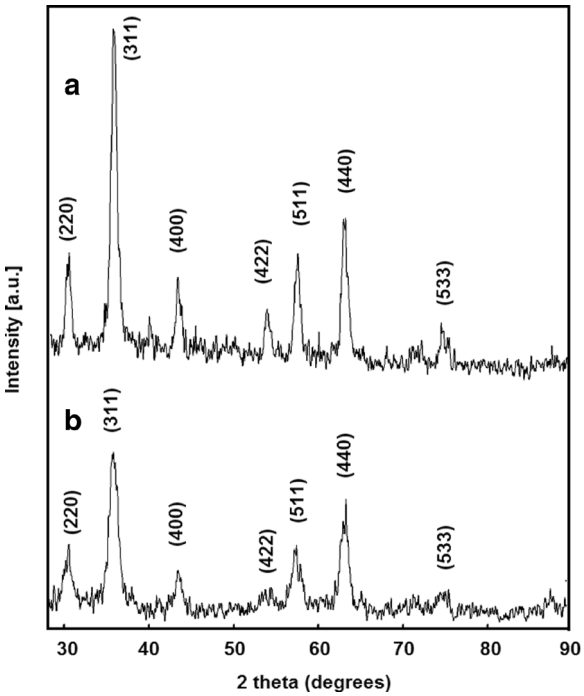

Fig. 2 X-ray diffraction (XRD) patterns for two selected polyol-coated SPION samples. **a** TREG-1. **b** PEG-1

corresponding polyol (TREG or PEG) coating over the Fe_3O_4 core was confirmed by FTIR. Figure 3 shows a comparison of the FTIR spectra for the TREG-2 and PEG-2 samples. As anticipated, the bands associated with the typical vibrational frequencies expected for PEG or TREG were found on the coated magnetic nanoparticles. Characteristic bands at 1140 cm^{-1} (C–O–C stretching vibration) and 1630 cm^{-1} (carboxyl band) corresponding to the PEG-coated nanoparticles are present, indicating their presence on the SPION crystal surface. These bands shifted towards lower wave number, in comparison with the bands corresponding to the free polyol and uncoated NPs (Fig. 3a). The same was found for TREG-coated SPIONs, where stretching bands at 1120, 1180 (C–O–C stretching vibration), and 1635 cm^{-1} (asymmetric COO stretching) were found, also shifted to lower energies compared to free TREG (Fig. 3b). The changes in vibrational frequencies can be related to the interaction of carboxylate (–COOH) groups and the SPIONs surface (Piñeiro-Redondo et al. 2011). The PEG or TREG coatings absorbed on the surface may help to stabilize the nanoparticles in aqueous suspensions, even under physiological conditions.

In vitro MRI experiments and relaxivity measurements Surface coating affects the magnetization of nanoparticles by modifying surface spin disorders and also modulates MRI relaxivity of nanoparticles by altering the diffusion of water molecules between the solution phase and the adjacent layer surrounding the particle surface (Ge et al. 2009). Magnetic resonance images in a lab-made *phantom* were recorded on a Philips 1.5 T MRI clinical imaging system at room temperature (~300 K). The images were taken in 2D with mFFE sequence with echo times TE = 0, 20, 40, 60, 80, and 100 ms at the same anatomical position (Fig. 4).

Transverse relaxation time T_2 (measured in ms) is associated with the transverse relaxation, where nuclear spins precession cease, thus losing their transverse magnetization (at the *xy* plane) after a radiofrequency pulse. This gap is produced by direct interaction between pairs of spins and therefore is called *spin-spin* relaxation. To determine the relaxometry of the samples, the decay of signal intensity S was fitted into the exponential Eq (1) (Papakonstantinou et al. 1995). The spin-echo sequence can be used to obtain an accurate measurement of T_2 relaxation time or the relaxation rate $R_2 = 1/T_2$. Some studies in vivo (He et al. 2012; Lind et al. 2002) and in vitro (Clark et al. 2003) have demonstrated a high degree of correlation between iron concentration and R_2 in biological tissues. Figure 4 shows how the T_2-weighted images change drastically in signal intensity when the amount of polyol-coated magnetic nanoparticles is increased. This change in intensity can be observed in the observed exponential decay curves for the different concentrations of samples TREG-1, PEG-1, TREG-2, and PEG-2 (Fig. 5).

Figure 4 clearly shows that the prepared SPIONs are able to generate MR contrast on transverse (T_2) proton relaxation times weighted sequences. Their r_2 relaxivities were obtained by calculating the slope of the plots of their relaxation rates, $1/T_2$, (in s^{-1}) versus Fe concentration (in mM), obtaining values of 205 mM^{-1} s^{-1} for TREG-1, 245 mM^{-1} s^{-1} for PEG-1, 227 mM^{-1} s^{-1} for TREG-2, and 257 mM^{-1} s^{-1} for PEG-2. Superparamagnetic magnetite nanoparticles with diameters ranging from 3 to 6 nm, coated with diethylene glycol or PEG, had r_2 relaxation rates from 29 to 119 mM^{-1} s^{-1} (Hu et al. 2010). Although it has been reported that superparamagnetic, monodispersed TREG-coated magnetite nanoparticles with sizes in the range of 8–9 nm, can act both as T_1 and T_2 contrast agents, their large r_2 value

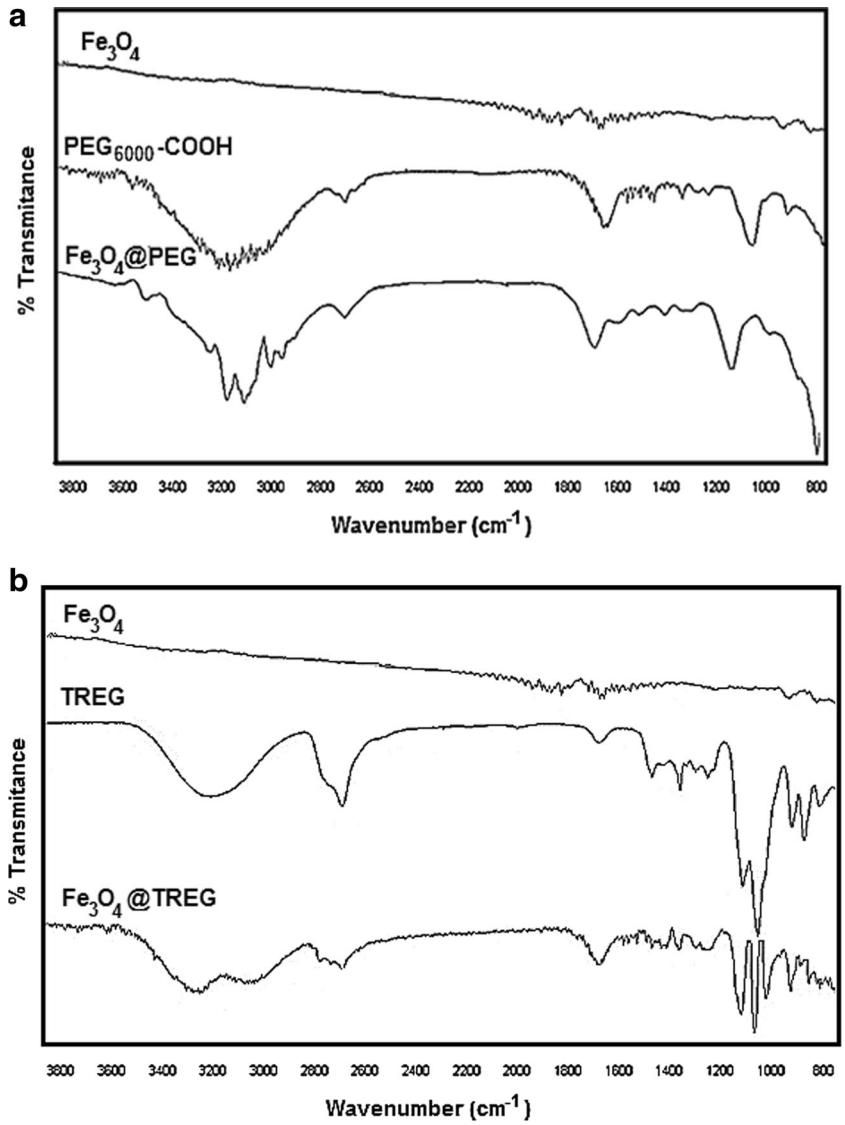

Fig. 3 FTIR spectra of (**a**) PEG- and (**b**) TREG-coated SPIONs, compared with pure samples of PEG and TREG

make them more suitable as T_2 contrast agents (Ma et al. 2010). The calculated small r_2 values for some of the SPIONs presented in this work might be useful for the development of $T_1 + T_2$ dual-contrast agents at clinically relevant magnetic fields (Hu et al. 2011). In this work, the lowest r_2 value of the four samples tested corresponds to TREG-1 (205 mM^{-1} s^{-1}); this is still higher than that of commercially available CA such as Feridex, Resovist, or Endorem that have r_2 values of 98.3, 151.0, and 189 mM^{-1} s^{-1}, respectively (Branca et al. 2015; Wang 2011), which makes all of these formulations good candidates for T_2 contrast agents.

The magnetization curves of TREG-2 and PEG-2 at 300, 100, and 10 K obtained by VSM are shown in Fig. 6. The magnetic hysteresis loops show a superparamagnetic behavior. The room temperature saturation magnetization values, M_s, for the two samples are 53 and 33 emu g^{-1}, respectively. M_s values in the 30 to 80 emu g^{-1} range have been reported in the literature and are typical for nanostructured Fe_3O_4 (Wu et al. 2008). No hysteresis in the magnetization curve and very small values in coercivity indicate that these SPIONs are superparamagnetic, as can be expected for MNPs of these sizes. Values of M_s without the contribution of TREG and PEG can be found in the Supplementary Information section.

As the hysteresis curves shows, sample TREG-2 presented higher M_s than PEG-2 even although PEG-

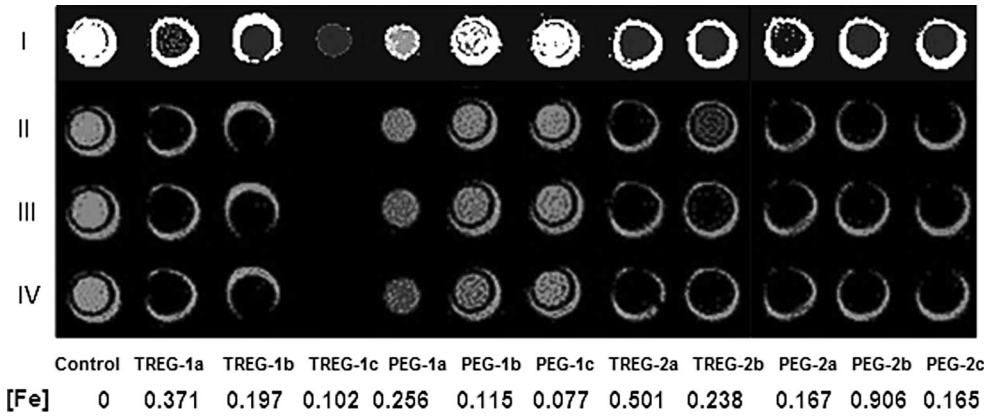

Fig. 4 T_2-weighted MR images of agar suspensions of TREG-1a, TREG-1b, TREG-1c, TREG-2a, TREG-2b and PEG-1a, PEG-1b, PEG-1c, PEG-2a, PEG-2b, PEG-2c SPIONs at different Fe concentrations (in mM). Images were taken at a cut to zero echo time (*I*) TE = 0 ms; (*II*) TE = 20 ms; (*III*) TE = 40 ms; (*IV*) TE = 60 ms

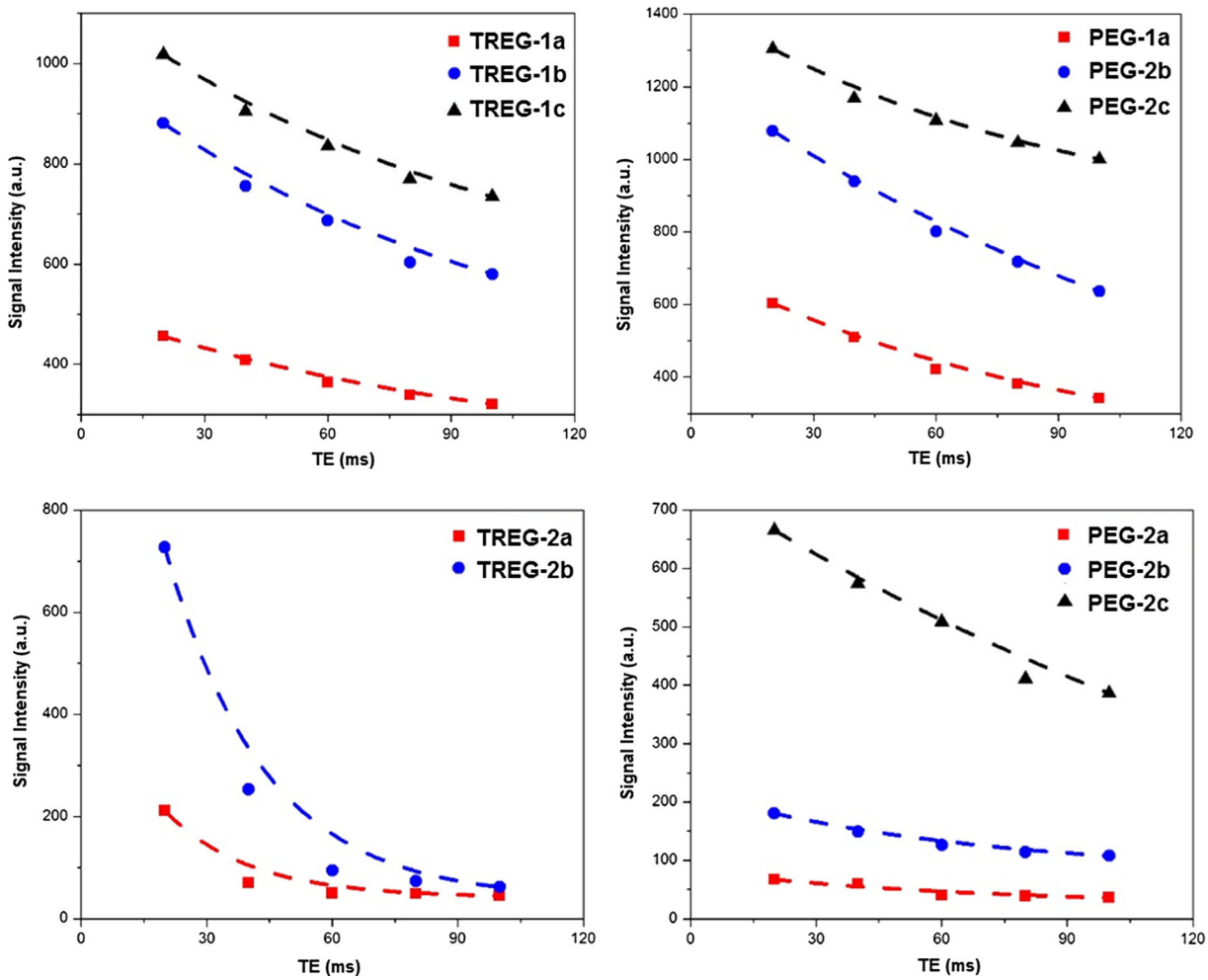

Fig. 5 Decay of the signal intensity of (**a**) TREG-1, (**b**) PEG-1, (**c**) TREG-2, (**d**) PEG-2 at different Fe concentrations (mM): TREG-1a, 0.371; TREG-1b, 0.197; TREG-1c, 0.102; PEG-1a, 0.256; PEG-1b, 0.115; PEG-1c, 0.077; TREG-2a, 0.501; TREG-2b, 0.238; PEG-2a, 0.167; PEG-2b, 0.906; PEG-2c, 0.165

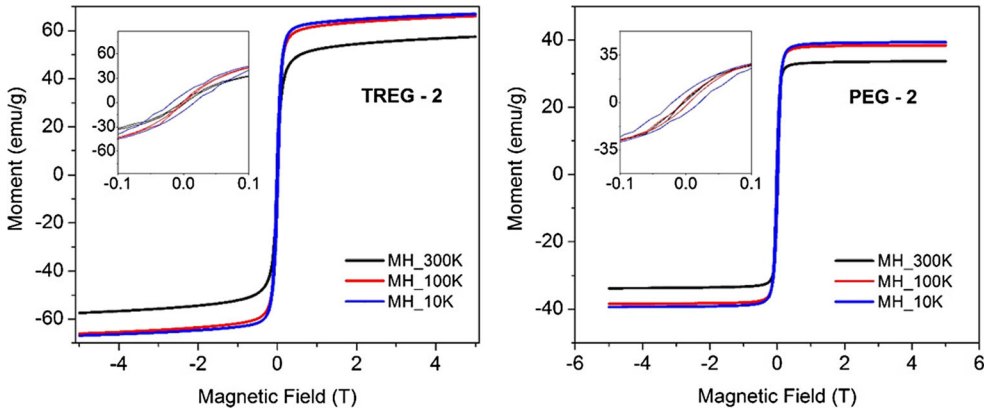

Fig. 6 Magnetization curves as obtained for TREG-2 and PEG-2 at 300, 100, and 10 K

coated nanoparticles were larger than TREG nanoparticles; this difference could be attributed mainly to the coating; since PEG has a larger hydrocarbon chain, the nanoparticles were more separated and synergic effects among the magnetic nanoparticles like dipolar coupling decrease their intensity resulting in lower M_s. This can also be seen with the HDD, where sample PEG-2 had the largest value compared to the rest of the samples (de la Presa et al. 2015; Arteaga-Cardona et al. 2016a).

Cell viability, histology, and in vivo MRI evaluation The effects of magnetic core-shell structure of the nanoparticles on fibroblast cell cultures were evaluated using contrast phase microscopy at 24 and 72 h after treatment. Fibroblast cells exposed to TREG-2 or PEG-2 nanoparticles maintained their normal morphology at the highest doses evaluated (160 μg/mL) after 72 h (Fig. SI-7b-e) and were not different from untreated control cells (Fig. SI-7a).

The dose and time response of core-shell magnetic nanoparticles were tested using the MTT viability test. The obtained data reveals that fibroblast cells remained viable after treatment with TREG or PEG-coated Fe_3O_4 nanoparticles in all the concentrations and times evaluated (Fig. 7). Very low toxicity was observed, even at high concentrations of TREG-2 or PEG-2 nanoparticles (160 μg/mL), which did not result in a significant difference in viability with respect to controls. These results are in agreement with previous works (Jia et al. 2012; Kim et al. 2006a, b). However, Gupta and Wells reported that functionalized magnetic nanoparticles reduced fibroblast viability by about 25–50% at concentrations in the range of 250 μg/mL (2004). In the present study, no significant changes in cell viability were observed even at the highest concentration used (160 μg/mL). Although morphological changes were observed in the cells treated with TREG-2, the viability of the cells was not affected thus suggesting biocompatibility. The observed biocompatibility of these polyol-coated *core-shell* magnetic nanoparticles, as well as their higher M_s (allowing for a reduced dosage of the CA), suggests that these NPs may potentially cause fewer adverse side effects and would be appropriate contrast agents for MRI and other biomedical uses.

Our results concur with the data we had reported previously that showed the effects on cell lines of magnetic nanoparticles functionalized with α-tocopheryl succinate (α-TOS-NPs); no significant effects on fibroblast cell cultures were found (Angulo-Molina et al. 2014). In that study, the internalization of the functionalized magnetic nanoparticles was proven by confocal microscopy analysis of FITC labeled nanoparticles. The precise mechanism of internalization for TREG and PEG-coated magnetic nanoparticles is still unknown, but it may be mediated by endo- and pinocytosis (Berry 2005). The MTT results are also in agreement with other previous studies (Anderson et al. 2004; Kim et al. 2006a).

As the obtained results, were in agreement with previous works reporting that Fe_3O_4 nanoparticles have low toxicity and no significant side effects when used as MRI contrast agents (Liu et al. 2013; Roper 1988), we proceeded to evaluate the in vivo biodistribution and MRI performance of one of the formulations in a rabbit. The TREG-2 sample was chosen as the contrast agent as it showed the highest M_s.

A suspension of 10 mg/mL (based on Fe concentration) of TREG-2 nanoparticles with core size in the

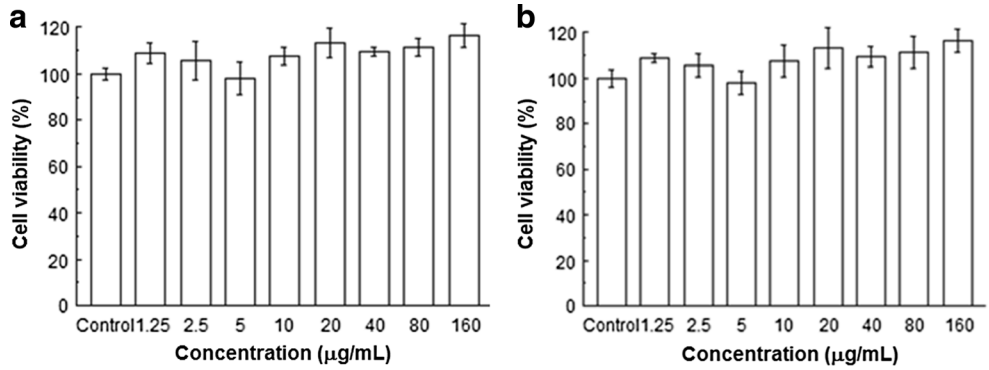

Fig. 7 Cell viability after 48 h for the samples. **a** TREG-2. **b** PEG-2. Fibroblast cells were treated with core-shell magnetic nanoparticles at different doses (0–160 μg/mL) for 48 h. The core-shell magnetic nanoparticles are biocompatible with fibroblast cells

range of 12 nm and a hydrodynamic diameter of 40 nm was injected intravenously into a rabbit's right ear vein, in a dose lower than that used for typical SPIONs based common MRI contrast agents (i.e., 28 mg/mL for Resovist™ for patients weighing less than 60 kg) (Wang 2011). It showed a negative enhancement effect, typical of a T_2 magnetic contrast agent as observed in Fig. 8, where the MRI image before injection (Fig. 8a) is compared to the T_2-weighted images for 3 days consecutive days after injection.

As shown in Fig. 9, the histopathological characteristics of tissues extracted from different organs after

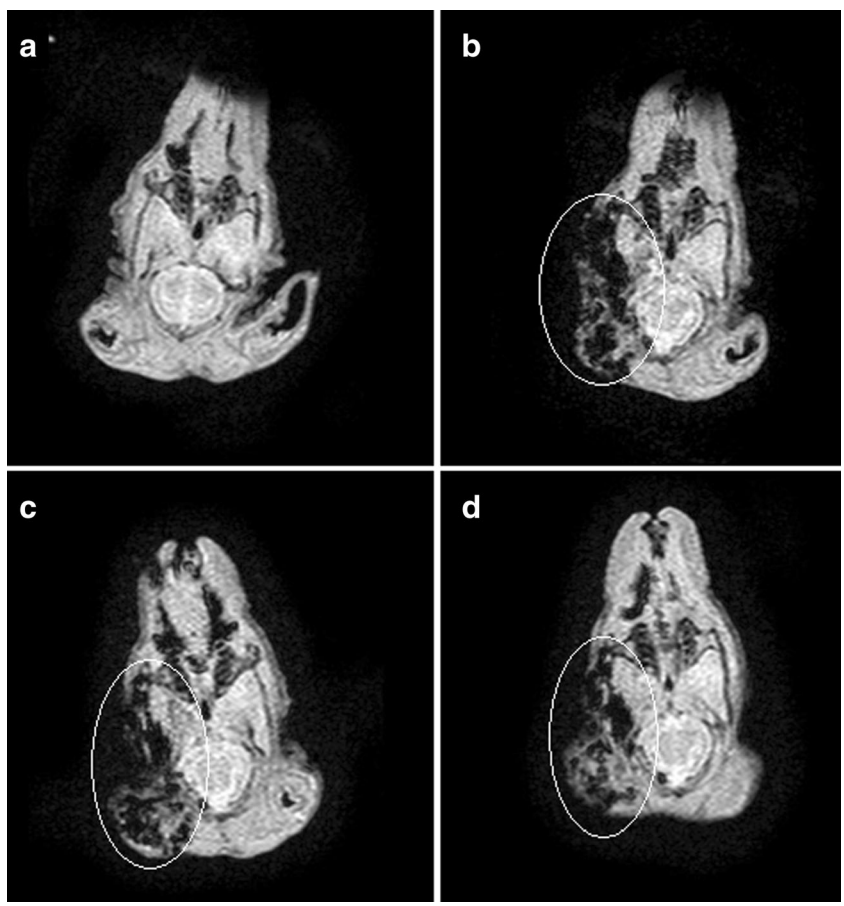

Fig. 8 MRI T_2-weighted images (TR/TE of 2348 ms/4.6 ms) at (**a**) pre-injection and (**b**) 1, (**c**) 2, and (**d**) 3 days post-injection with TREG-2 nanoparticles (10 mg Fe/kg body weight) by IV administration. The magnetic nanoparticles accumulation zones are *circled*

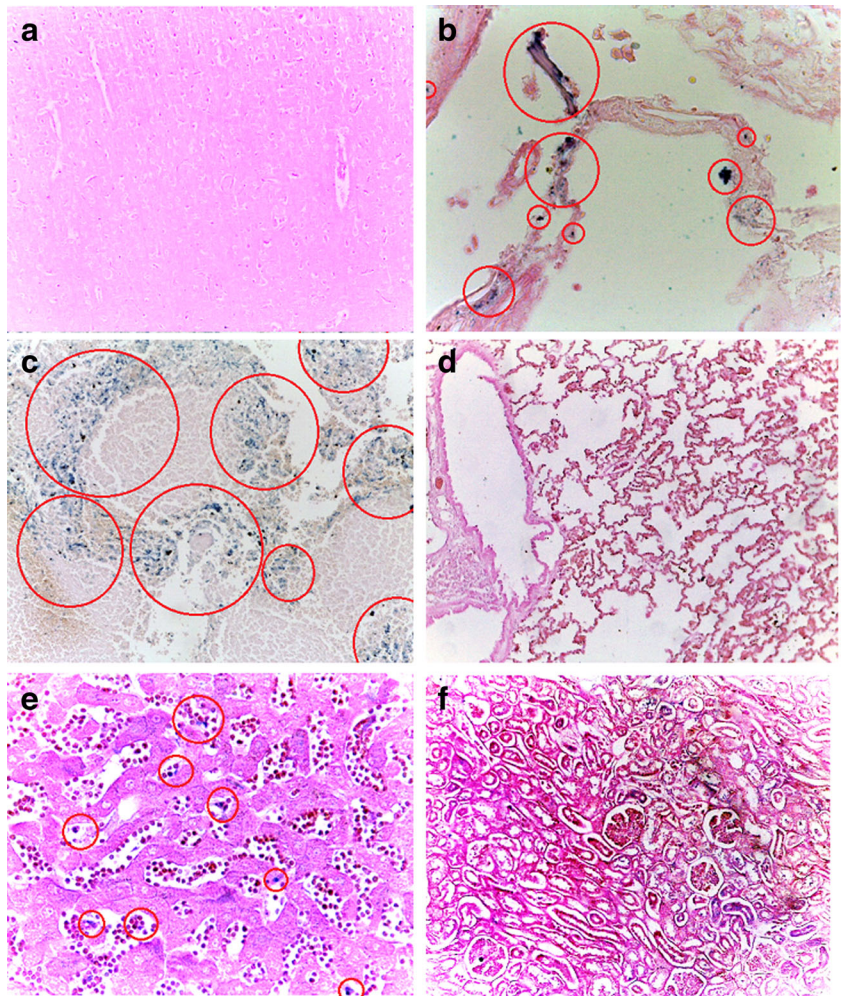

Fig. 9 Histopathological analysis of tissue slices after hematoxylin-eosin and Prussian blue staining. **a** Brain. **b** Meninges. **c** Spleen. **d** Lungs. **e** Liver. **f** Kidney. Identification of TREG-2 nanoparticles as blue clusters is *circled*. ×10 magnification, light microscope

staining with hematoxylin-eosin did not show any sign of structural change indicative of cell or tissue damage. As the TREG-2 nanoparticles contain iron ions, their distribution can be examined using Prussian blue staining of tissues from the selected organs. This method is highly selective for exogenous iron, and although the liver and spleen normally accumulate iron and show positive results to the Prussian blue staining, the accumulation of exogenous iron yields a more intense blue color. No significant blue colors were found in tissue samples from the esophagus, heart, lung, and kidney, neither was there any detectable change in typical tissue morphology, which suggests that TREG-2 nanoparticles are non-toxic and do not accumulate in those organs. Positive results, indicated as blue-stained particle clusters, were found mainly in the meninges, spleen, and liver, suggesting that the nanoparticles are being handled by the RES system. These results indicate that the TREG-2 nanoparticles have good tissular diffusion, large half-life values, and distribute through the systemic circulation before being sequestered by the RES system (Jia et al. 2012). The dark regions correspond to zones around the brain, histologically identified as the meninges, associated with the accumulation of TREG-2 nanoparticles after biodistribution and clearance by the RES. The MR images show that the T_2 contrast is mainly located outside of the brain parenchyma, indicating that the nanoparticles accumulated in the blood vessels around the meningeal tissue but did not cross the blood brain barrier (BBB).

Although most nanoparticles are unable to cross the BBB, engineered magnetic nanoparticles may reach the brain after intravenous, intraperitoneal, or inhalation administration (Kim et al. 2006b; Kong et al. 2012;

Kwon et al. 2008; Liu et al. 2013). It has been reported that SPIONs coated with the polysaccharide dextran, commonly used as MRI contrast agents, are able to cross the BBB and are neuro-biocompatible (Kim et al. 2006b; Kong et al. 2012; Kwon et al. 2008; Liu et al. 2013; Roper 1988).

Conclusions

In this work, we used the polyol process to create a system with characteristics apt for biomedical applications such as MRI contrast agents. We had seen favorable reports of polyol synthesis (especially for PEG and TREG) showing that this one-step cost-effective method produces NPs that are of uniform size, with narrow dispersibility, biocompatible, and water soluble, all essential characteristics for CAs. Modifying the experimental conditions, thermal decomposition, iron precursor, surfactant, solvent, reaction temperature, and time, allowed us to control the size and resulting magnetism of the NPs. Two types of water-dispersible magnetite (Fe_3O_4)-based SPIONs, surface coated and stabilized with carboxylated polyethylene glycol 6000 (PEG-1 and PEG-2) or triethylene glycol (TREG-1 and TREG-2), were obtained by a simple one-step reaction. Their average hydrodynamic sizes were in the 20 to 180 nm range, while their TEM estimated sizes were in the 6 to 14 nm range. The resulting nanoparticles were highly crystalline and stable at pH 7 in water. Acquisition of MR images and analysis of the obtained data fit on an exponential behavior curve shows that their T_2 relaxation times are influenced both by their size and the polyol and Fe concentrations used in the preparation of the NPs. In addition to their stability and their low tendency to agglomerate in solution, the sizes of these SPIONs are small enough to avoid uptake by cells of the RES and big enough to avoid rapid renal clearance. The Fe concentrations evaluated in this work were lower than those reported previously for other SPIONs coated with a bipolar surfactant (tetramethylammonium-11-aminoundecanoato), where their biological activity against normal glial and breast cancer cells was determined to become toxic at concentrations higher than 100 μg/mL^2. The in vitro cytotoxicity test against fibroblast cells showed that both the TREG and PEG-coated core-shell Fe_3O_4 magnetic nanoparticles are non-toxic and biocompatible. All the prepared polyol-coated SPIONs responded well as magnetic CAs in agar phantoms in vitro experiments, and one of them, TREG-2, was evaluated in vivo in a rabbit, showing good performance as a T_2 contrast agent and good biodistribution in the liver, spleen, and meninges. The MRI is considered a highly sensitive clinical diagnosis technique (i.e., pathologic conditions are easily shown). The development of better CAs may help to improve their specificity and, as reported here, SPIONs with lower concentrations of Fe may reduce potential side effects in the patients. Further work is currently underway on this topic.

Acknowledgements This work was supported by CONACYT (Grants # CB-2010/154602 and CB-2010/151767) and the Welch Foundation (Grant P-1212). SHT thanks Hospital Infantil de México Federico Gómez for access to its clinical MRI facilities. We would like to thank Dr. María Eugenia Mendoza (Instituto de Física, BUAP) for the XRD analysis of the samples. We would also like to express our gratitude to Rachel M. West (rmartwest@gmail.com) for the English editing, scientific comments, and correction of this manuscript.

Compliance with ethical standards All applicable international, national, and/or institutional guidelines for the care and use of animals were followed.

Funding This study was funded by CONACYT (grant number CB-2010/154,602 and CB-2010/151,767) and the Robert A. Welch Foundation (grant number P-1212).

Conflict of interest The authors declare that they have no conflict of interest.

References

Ali A, Zafar H, Zia M, Haq I, Rehman A et al (2016) Synthesis, characterization, applications and challenges of iron oxide nanoparticles. Nanotechnol Sci Appl 9:49–67

Ammar S, Helfen A, Jouini N, Fievet F, Roserman I et al (2001) Magnetic properties of ultrafine cobalt ferrite particles synthesized by hydrolysis in a polyol medium. J Mater Chem 11: 186

Anderson K, Simmons-Menchaca M, Lawson KA, Atkinson J, Sanders BG et al (2004) Differential response of human ovarian cancer cells to induction of apoptosis by vitamin E succinate and vitamin E analogue, alpha-TEA. Cancer Res 64:4263–4269

Angulo-Molina A, Mendez-Rojas MA, Palacios-Hernandez T, Contreras-Lopez OE, Hirata-Flores GA, Flores-Alonso JC, Merino-Contreras S, Valenzuela O, Hernandez J, Reyes-Leyva J (2014) Magnetite nanoparticles functionalized with α-tocopheryl succinate (α-TOS) promote selective cervical cancer cell death. J Nanopart Res 16:2528

Arteaga-Cardona F, Rojas-Rojas K, Costo R, Mendez-Rojas MA, Hernando A, de la Presa P (2016a) Improving the magnetic heating by disaggregating nanoparticles. J Alloys Compd 663:636

Arteaga-Cardona F, Santillán-Urquiza E, de la Presa P, Tobón SH, Pal U, Horta-Fraijo P, José-Yacaman M, Lozada-Ramírez JD, Ivkov R, Angulo-Molina A, Méndez-Rojas MA (2016b) Enhanced magnetic properties and MRI performance of bi-magnetic core–shell nanoparticles. RSC Adv 6:77558

Beltran-Huarac J, Guinel MJF, Weiner BR, Morell G (2013) Bifunctional Fe_3O_4/ZnS:Mn composite nanoparticles. Mater Lett 98:108

Berry CC (2005) Possible exploitation of magnetic nanoparticle-cell interaction for biomedical applications. J Mater Chem 15:543–547

Bourrinet P, Bengele HH, Bonnemain B, Dencausse A, Idee JM et al (2006) Preclinical safety and pharmacokinetic profile of ferumoxtran-10, an ultrasmall superparamagnetic iron oxide magnetic resonance contrast agent. Investig Radiol 41:313–324

Branca M, Marciello M, Ciuculescu-Pradines D, Respaud M, Morales MP, Serra R, Casanove MJ, Amiens C (2015) Towards MRI T_2 contrast agents of increased efficiency. J Magn Magn Mater 377:348

Cai W, Wan J (2007) Facile synthesis of superparamagnetic magnetite nanoparticles in liquid polyols. J Colloid Interface Sci 305:366–370

Clark PR, Chua-Anusorn W, St Pierre TG (2003) Proton transverse relaxation rate (R_2) images of liver tissue; mapping local tissue iron concentrations with MRI [corrected]. Magn Reson Med 49:572–575

de la Presa P, Luengo Y, Velasco V, Morales MP, Iglesias M, Veintemillas-Verdaguer S, Crespo P, Hernando A (2015) Particle interactions in liquid magnetic colloids by zero field cooled measurements: effects on heating efficiency. J Phys Chem C 119:11022

de Oliveira CC, Ando RA, Camargo PH (2013) Size-controlled synthesis of silver micro/nanowires as enabled by HCL oxidative etching. Phys Chem Chem Phys 15:1887–1893

Engelhardt R, Langkowski JH, Fischer R, Nielsen P, Kooijman H et al (1994) Liver iron quantification: studies in aqueous iron solutions, iron overloaded rats, and patients with hereditary hemochromatosis. Magn Reson Imaging 12:999–1007

Feldmann C, Jungk HO (2001) Polyol-mediated preparation of nanoscale oxide particles. Angew Chem Int Ed Engl 40:359–362

Fishman A, Acton A, Lee-Ruff E (2004) A simple preparation of PEG-carboxylates by direct oxidation. Synth Commun 34: 2309–2312

Gao J, Gu H, Xu B (2009) Multifunctional magnetic nanoparticles: design, synthesis, and biomedical applications. Acc Chem Res 42:1097–1107

Ge YQ, Zhang Y, Gu N et al (2009) Effect of surface charge and agglomerate degree of magnetic iron nanoparticles on KB cellular uptake in vitro. Colloid Surface B 73:294–301

Ghotbi MY, bin Huessein MZ (2012) Controlled release study of an anti-carcinogenic agent, gallate from the surface of magnetite nanoparticles. J Phys Chem Solids 73:936–942

Gupta AK, Wells S (2004) Surface-modified superparamagnetic nanoparticles for drug delivery: preparation, characterization, and cytotoxicity studies. IEEE Trans Nanobioscience 3:66–73

Hachani R, Lowdell M, Birchall M, Hervault A, Mertz D, Begin-Colin S, Thanh NTK (2016) Polyol synthesis, functionalization and biocompatibility studies of superparamagnetic iron oxide nanoparticles as potential MRI contrast agents. Nanoscale 8: 3278

He Q, Wu Z, Huang C (2012) Hollow magnetic nanoparticles: synthesis and applications in biomedicine. J Nanosci Nanotechnol 12:2943–2954

Hu F, Joshi HM, Dravid VP, Meade TJ (2010) High-performance nanostructured MR contrast probes. Nanoscale 2:1884–1891

Hu F, Jia Q, Li Y, Gao M (2011) Facile synthesis of ultrasmall PEGylated iron oxide nanoparticles for dual-contrast T_1- and T_2-weighted magnetic resonance imaging. Nanotechnology 22:245604

Issa B, Obaidat IM, Albiss BA, Haik Y (2013) Magnetic nanoparticles: surface effects and properties related to biomedicine applications. Int J Mol Sci 14:21266

Jia Y, Yuan M, Yuan H, Huang X, Sui X et al (2012) Co-encapsulation of magnetic Fe3O4 nanoparticles and doxorubicin into biodegradable PLGA nanocarriers for intratumoral drug delivery. Int J Nanomedicine 7:1697–1708

Jiang L, Li X, Liu L, Zhang Q (2013) Thiolated chitosan-modified PLA-PCL-TPGS nanoparticles for oral chemotherapy of lung cancer. Nanoscale Res Lett 8:66

Joseyphus RJ, Shinoda K, Kodama D, Jeyadevan B (2010) Size controlled Fe nanoparticles through polyol process and their magnetic properties. Mater Chem Phys 123:487

Kim DH, Lee SH, Im KH, Kim KN, Kim KM et al (2006a) Surface-modified magnetite nanoparticles for hyperthermia: preparation, characterization, and cytotoxicity studies. Curr Appl Phys 6. Supplement 1:e242–e246

Kim JS, Yoon TJ, Yu KN, Kim BG, Park SJ et al (2006b) Toxicity and tissue distribution of magnetic nanoparticles in mice. Toxicol Sci 89:338–347

Kong SD, Lee J, Ramachandran S, Eliceiri BP, Shubayev VI et al (2012) Magnetic targeting of nanoparticles across the intact blood-brain barrier. J Control Release 164:49–57

Kwon JT, Hwang SK, Jin H, Kim DS, Minai-Tehrani A et al (2008) Body distribution of inhaled fluorescent magnetic nanoparticles in the mice. J Occup Health 50:1–6

Lind K, Kresse M, Debus NP, Muller RH (2002) A novel formulation for superparamagnetic iron oxide (SPIO) particles enhancing MR lymphography: comparison of physicochemical properties and the in vivo behaviour. J Drug Target 10: 221–230

Liu G, Gao J, Ai H, Chen X (2013) Applications and potential toxicity of magnetic iron oxide nanoparticles. Small 9:1533–1545

Ma Y, Zheng Y, Liu K, Tian G, Tian Y et al (2010) Nanoparticles of poly(Lactide-Co-Glycolide)-d-α-tocopheryl polyethylene glycol 1000 succinate random copolymer for cancer treatment. Nanoscale Res Lett 5:1161–1169

Masala O, Seshadri R (2005) Magnetic properties of capped, soluble $MnFe_2O_4$ nanoparticles. Chem Phys Lett 402:160

Merbach A, Helm L, Toth E (eds) (2001) The chemistry of contrast agents in medical magnetic resonance imaging. Wiley, Chichester

Miguel-Sancho N, Bomati-Miguel O, Colom G, Salvador JP, Marco MP, Santamaria J (2011) Development of stable, water-

dispersible, and biofunctionalizable superparamagnetic iron oxide nanoparticles. Chem Mater 23:2795

Mondini S, Cenedese S, Marioni G, Molteni G, Santo N et al (2008) One-step synthesis and functionalization of hydroxyl-decorated magnetite nanoparticles. J Colloid Interface Sci 322:173

Mornet S, Vasseur S, Grasset F, Duquet E (2004) Magnetic nanoparticle design for medical diagnosis and therapy. J Mater Chem 14:2161–2175

National Research Council (2011) Guide for the Care and Use of Laboratory Animals 8th edn. National Academies Press, Washington, DC

OsiriX (2004) An open source software for navigation in multidimensional DICOM images. J Digit Imaging 17:205–216

Panagiotopoulos N, Duschka RL, Ahlborg M, Bringout G, Debbeler C et al (2015) Magnetic particle imaging: current developments and future directions. Int J Nanomedicine 10: 3097–3114

Pankhurst QA, Connolly J, Jones SK, Dobson J (2003) Applications of magnetic nanoparticles in biomedicine. J Phys D Appl Phys 36:R167

Papakonstantinou OG, Maris TG, Kostaridou V, Gouliamos AD, Koutoulas GK et al (1995) Assessment of liver iron overload by T_2-quantitative magnetic resonance imaging: correlation of T_2-QMRI measurements with serum ferritin concentration and histologic grading of siderosis. Magn Reson Imaging 13: 967–977

Piñeiro-Redondo Y, Bañobre-López M, Pardiñas-Blanco I, Goya G, López-Quintela MA, Rivas J (2011) The influence of colloidal parameters on the specific power absorption of PAA-coated magnetite nanoparticles. Nanoscale Res Lett 6: 383

Pisciotti MLM, Lima E, Vasquez Mansilla M, Tognoli VE, Troiani HE, Pasa AA, Creczynski-Pasa TB, Silva AH, Gurman P, Colombo L, Goya GF, Lamagna A, Zysler RD (2016) In vitro and in vivo experiments with iron oxide nanoparticles functionalized with DEXTRAN or polyethylene glycol for medical applications: magnetic targeting. J Biomed Mat Res B Appl Biomat 102:860–868

Rohani Moghadam M, Haji Shabani AM, Dadfarnia S (2015) Simultaneous spectrophotometric determination of Fe(III) and Al(III) using orthogonal signal correction-partial least squares calibration method after solidified floating organic drop microextraction. Spectrochim Acta A Mol Biomol Spectrosc 135:929–934

Rojas-Perez A, Diaz-Diestra D, Frias-Flores CB, Beltran-Huarac J, Das KC, Weiner BR, Morell G, Diaz-Vazquez LM (2015) Catalytic effect of ultrananocrystalline Fe_3O_4 on algal biocrude production via HTL process. Nanoscale 7:17664

Roper WL (1988) Shaping the future of American medicine. Ala J Med Sci 25:470–474

Santillán-Urquiza E, Arteaga-Cardona F, Hernandez-Herman E, Pacheco-García PF, González-Rodríguez R, Coffer JL, Mendoza-Alvarez ME, Vélez-Ruiz JF, Méndez-Rojas MA (2015) Inulin as a novel biocompatible coating: evaluation of surface affinities toward $CaHPO_4$, α-Fe_2O_3, ZnO, $CaHPO_4$@ZnO and α-Fe_2O_3@ZnO nanoparticles. J Colloid Interface Sci 460:339

Sun P, Hui C, Azim Khan R, Du J, Zhang Q et al (2015) Efficient removal of crystal violet using Fe_3O_4-coated biochar: the role of the Fe_3O_4 nanoparticles and modeling study their adsorption behavior. Sci Rep 5:12638

Wahajuddin, Sumit A (2012) Superparamagnetic iron oxide nanoparticles: magnetic nanoplatforms as drug carriers. Int J Nanomedicine 7:3445

Wang YX (2011) Superparamagnetic iron oxide based MRI contrast agents: current status of clinical application. Quant Imaging Med Surg 1:35–40

Wang LM, Song C, Jin J (1982) Spectrophotometric determination of iron with 1,10-phenanthroline in the presence of copper. Microchim Acta 78:115–124

Wang Z, Zhu H, Wang X, Yang F, Yang X (2009) One-pot green synthesis of biocompatible arginine-stabilized magnetic nanoparticles. Nanotechnology 20:465606

Wei C, Wan J (2007) Facile synthesis of superparamagnetic magnetite nanoparticles in liquid polyols. J Colloid Interface Sci 305:366

Weissleder R, Stark DD, Engelstad BL, Bacon BR, Compton CC et al (1989) Superparamagnetic iron oxide: pharmacokinetics and toxicity. Am J Rentgenol 152:167

Weissleder R, Elizondo G, Wittenberg J, Rabito CA, Bengele HH et al (1990) Ultrasmall superparamagnetic iron oxide: characterization of a new class of contrast agents for MR imaging. Radiology 175:489–493

Witter R, Roming M, Feldmann C, Ulrich AS (2013) Multilayered core-shell structure of polyol-stabilized calcium fluoride nanoparticles characterized by NMR. J Colloid Interface Sci 390:250–257

Wu W, He Q, Jiang C (2008) Magnetic iron oxide nanoparticles: synthesis and surface functionalization strategies. Nanoscale Res Lett 3:397–415

Xue S, Zhang C, Yi Y, Zhang L, Dengfeng C, Zhang J, Shi H, Zhang Y (2015) ^{99m}Tc-labeled iron oxide nanoparticles for dual-contrast (T_1/T_2) magnetic resonance and dual-modality imaging of tumor angiogenesis. J Biomed Nanotech 11:1027

Yallapu MM, Foy SP, Jain TK, Labhasetwar V (2010) PEG-functionalized magnetic nanoparticles for drug delivery and magnetic resonance imaging applications. Pharm Res 27: 2283–2295

Yang K, Feng L, Hong H, Cai W, Liu Z (2013) Preparation and functionalization of graphene nanocomposites for biomedical applications. Nat Protoc 8:2392–2403

Zhang DH, Li GD, Li JX, Chen JS (2008) One-pot synthesis of Ag-Fe_3O_4 nanocomposite: a magnetically recyclable and efficient catalyst for epoxidation of styrene. Chem Commun 29:3414–3416

Zhang L, Dong WF, Sun HB (2013) Multifunctional superparamagnetic iron oxide nanoparticles: design, synthesis and biomedical photonic applications. Nanoscale 5:7664

Zhu L, Torchilin VP (2013) Stimulus-responsive nanopreparations for tumor targeting. Integr Biol 5:96–107